JOURNAL OF THERMOPHYSICS AND HEAT TRANSFER
Vol. 7, No. 3, July–Sept. 1993

Numerical Solution of Axisymmetric Heat Conduction Problems Using Finite Control Volume Technique

B. F. Blackwell* and R. E. Hogan†
Sandia National Laboratories, Albuquerque, New Mexico 87185

A finite control volume technique is developed to solve two-dimensional axisymmetric heat conduction problems using an arbitrary quadrilateral mesh. In this technique, the integral form of the conservation of energy equation is applied to control volumes of finite size. The boundary conditions considered include specified flux, aerodynamic heating, convection, and radiation. Two example problems involving a specified heat flux boundary condition and a specified temperature in conjunction with a temperature-dependent source are presented to demonstrate quadratic convergence as the mesh is spatially refined. The temperature-dependent source problem is solved using both a rectangular and a skewed mesh; the method is capable of producing accurate results on both rectangular and skewed meshes. Numerical comparisons with a Galerkin finite element code are also presented.

Nomenclature

C_h = aerodynamic heating transfer coefficient
C_{ij} = elements of the element capacitance matrix
C_p = constant pressure specific heat
CS = control surface
CV = control volume
$CV_i^{(e)}$ = partial control volume surrounding node i of element e
D = shape function derivative matrix
$d\boldsymbol{A}$ = differential area vector
$d\boldsymbol{S}$ = normal vector along control surface
E_i = elements of the element generation matrix
$\dot{e}'''$ = temperature-dependent volumetric source
F = radiative view factor
h = convective heat transfer coefficient
i_r = freestream recovery enthalpy for aerodynamic heating boundaries
i_w = gas enthalpy at the wall temperature for aerodynamic heating boundaries
J = Jacobian of the coordinate transformation
J_0 = Bessel function of the first kind of order zero
J_1 = Bessel function of the first kind of order one
K_{ij} = elements of the element conduction matrix
k = thermal conductivity
L = length of cylinder
N_i = element shape functions
$\boldsymbol{n}$ = unit vector
p = dimensionless generation, see Eq. (58)
$\dot{Q}$ = heat transfer rate
$\dot{\boldsymbol{q}}$ = heat flux vector
r = global radial coordinate
r_0 = cylinder radius
S_C = constant in the source term
$S_i^{(e)}$ = portion of the boundary of element e associated with node i
S_{ij} = boundary distance between nodes i and j
S_P = constant in the temperature-dependent source
T = temperature
t = time
z = global axial coordinate
α = thermal diffusivity, constant in source term
β_i = coefficients in element temperature profile
δ_{ij} = Kronecker delta
ε = surface emittance
η = local coordinate
ξ = local coordinate
ρ = density
σ = Stefan-Boltzmann constant
ψ = dimensionless temperature, see Eq. (58)

Subscripts

1, 2, 3, . . . = indices referring to nodes of control volume
a = refers to analytical results
aero = aerodynamic heating boundary conditions
c = refers to computed results
conv = convective boundary conditions
flux = specified flux boundary conditions
i, j = node number
r = in global r coordinate direction
rad = radiative boundary conditions
z = in global z coordinate direction

Superscripts

$e, e+1, \ldots$ = indices referring to elements
n = refers to last time step
$n+1$ = refers to current time step
T = transpose of matrix
-1 = inverse of matrix

Received July 10, 1991; revision received June 4, 1992; accepted for publication June 5, 1992.
*DMTS, Thermophysics Department 1553. Member AIAA.
†SMTS, Thermal and Fluid Engineering Department 1513.

I. Introduction

A. Control Volume Philosophy

A COMMON way of deriving the differential equations that describe physical phenomena is to apply conservation principles to a control volume of infinitesimal size and take the limit as the control volume shrinks to zero. When finite difference techniques are applied to solve these differential equations, we are undoing the limiting process of allowing the control volume to shrink to zero. The finite control

volume method (FCVM) applies the integral form of the conservation principles directly to control volumes of finite size. This approach starts from the exact form of the conservation principles. No approximations are necessary until an assumption is made about how the dependent variables (such as density, velocity, temperature, and pressure) vary with position and/or time; then, these integrals can be evaluated in terms of nodal variables. In assuming "profile" shapes, one can make use of as much physics as is known about the problem. For mathematical convenience, linear profiles are often assumed; however, one should seek a profile that best matches the physics. Admittedly, most things appear to be linear if they are observed on a sufficiently small scale. However, being forced to use a small scale means a greater number of unknown nodal variables for a given problem accuracy.

The FCVM presented here is a natural extension of the control volume concepts presented to students of engineering and physics. In fact, the method can be applied to the solution of field problems described by ordinary or partial differential equations without any knowledge of the formal solution techniques for these ordinary or partial differential equations. The integral form of the conservation principles can lead directly to algebraic (or ordinary differential) equations involving nodal variables without ever producing the ordinary (or partial) differential equations that describe the phenomena.

B. Literature Review

One of the first applications of control volumes with an unstructured mesh for the solution of diffusion problems was presented by Winslow.[1] In this work, the solution of the Poisson equation was obtained using a finite difference-based approach and a triangular mesh with polygon-shaped control volumes. The element-based FCVM approach for solving diffusion problems was developed by Baliga[2] for two-dimensional planar geometries using three-node linear triangles. In addition to diffusion problems, Baliga[2] extended the FCVM to solve both diffusion-convection and general fluid flow problems using triangular elements and a novel exponential interpolating polynomial that is sensitive to the local Peclet number. Independently, Hogan[3] and Hogan and Blackwell[4] developed a similar approach for two-dimensional planar and axisymmetric geometries using three-node triangular elements; problems with specified heat flux, convective, and radiative boundary conditions were analyzed. Ramadhyani and Patankar[5] solved the Poisson equation using four-node rectangular elements and a bilinear interpolating polynomial. Later, Schneider and Zedan[6] extended the method to two-dimensional planar geometries using arbitrary four-node quadrilaterals. The same concepts were extended by Raw et al.[7] using nine-noded quadrilaterals with quadratic interpolating polynomials. In the work presented here, the development of the FCVM using arbitrary four-node quadrilaterals is presented for two-dimensional axisymmetric geometries with anisotropic material properties. This development includes the appropriate contributions to account for specified heat flux, convective, radiative, and aerodynamic heating boundary conditions.

Accuracy comparisons of the FCVM and other solution methods show the promise of the approach. Ramadhyani and Patankar[5] compared the FCVM and the Galerkin Finite Element Method (FEM) solution for heat conduction in a rectangular bar both with and without uniform heat generation. The FCVM resulted in errors that were roughly 50% smaller than the Galerkin FEM errors. For steady-state radial heat conduction in a hollow cylinder, Schneider and Zedan[6] showed that the FCVM errors were at least as small as the Galerkin FEM, and in several cases up to 40% smaller. Additionally, estimates of savings in setting up the "stiffness" matrix were reported generally in excess of 25%. For the predominantly flux prescribed problem, Raw et al.[7] showed the FCVM results and the Galerkin FEM were similar. However, for the convective boundary conditions, a decrease in error of two orders of magnitude relative to the Galerkin FEM was reported. Banaszek[8] showed that the FCVM provided better accuracy than the Galerkin FEM for both a steady-state problem with anisotropic material properties and a transient nonlinear problem. Additionally, less stringent stability requirements for the FCVM were shown using a von Neumann type analysis. These aspects permit coarser meshes and larger time steps for similar accuracy. Additional details of the FCVM can be found in Ref. 9.

The application of the FCVM to heat conduction problems is a conceptually simple procedure, since it builds on the control volume approach taught in undergraduate engineering and physics courses. Kao[10] proposed that the FCVM using triangular elements and linear interpolating polynomials be included in undergraduate numerical methods courses. The FCVM has been taught in a senior level numerical methods course at Texas A&M University since 1982.[11]

II. Development of Discretized Equations for a Four-Node Quadrilateral Mesh

The algebraic equations representing conservation of energy in a heat conducting medium will be developed by applying the integral form of the conservation of energy equation to control volumes of finite size. Figure 1 is a schematic of an arbitrary quadrilateral mesh in which each quad has four nodes. The node and element numbering system is arbitrary; however, element e has nodes 1-2-3-4 numbered in a counterclockwise fashion (chosen for convenience and consistency). The control volume about node 3 is shown as the hashed region. In general, conservation of energy in a heat conducting solid for an arbitrary control volume can be written as

$$\frac{\partial}{\partial t}\int_{CV} \rho C_p T \, dV + \int_{CS} (d\boldsymbol{A}\cdot\dot{\boldsymbol{q}}) = \int_{CV} \dot{e}''' \, dV \qquad (1)$$

where ρC_p is the volumetric heat capacity, $\boldsymbol{A}$ is the area vector normal to the control volume boundary, and CS and CV represent integration over the surface and volume of the control volume, respectively. To develop an equation representing conservation of energy for the control volume surrounding node 3 in Fig. 1, each of the terms in Eq. (1) must be evaluated for the crosshatched control volume. For the control volume shown, the four elements e, . . . , e + 3 contribute to the energy balance on node 3; the analysis that follows is valid for an *arbitrary* number of elements contributing to a control volume.

In the finite difference approach to solving diffusion problems, algebraic equations are generally developed on a nodal

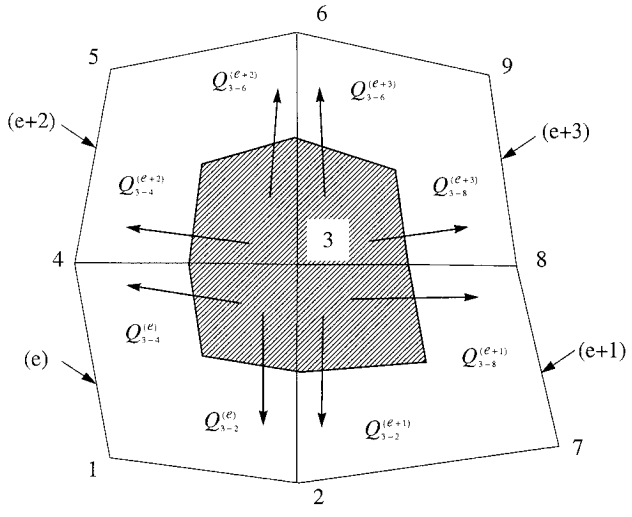

Fig. 1 Schematic of control volume surrounding node 3 and representation of conduction energy flux terms.

basis. In the FCVM, they are formulated on an element-by-element basis, similar to the FEM. Each quadrilateral element will have contributions to the portion of the control volume about each of its four nodes. In this article, the contribution of a typical element e to the partial control volume about each of the four nodes will be developed. This contribution is expressed in terms of element capacitance, conduction, and source matrices, corresponding to the three terms in Eq. (1). To develop the matrices that represent the elemental contribution to each control volume, consider the typical element e shown in Fig. 2. The contribution of this element to the control volume about node 3 will be explicitly developed. This will require explicit expressions for the net heat conducted $(\dot{Q}^{(e)}_{3-4} - \dot{Q}^{(e)}_{2-3})$ out of that portion of control volume 3 through the control surfaces and the energy storage and generation within $CV^{(e)}_3$. The subscript notation on $\dot{Q}^{(e)}_{i-j}$ is suggestive of conduction from node i to node j and $\dot{Q}^{(e)}_{i-j} = -\dot{Q}^{(e)}_{j-i}$. Before any of the integrals in energy balance Eq. (1) can be evaluated, it will be necessary to assume an element temperature profile.

A. Element Temperature Profile

Within each element, the temperature profile is assumed to be bi-linear in space

$$T(z, r) = \beta_0 + \beta_1 z + \beta_2 r + \beta_3 zr \tag{2}$$

where (z, r) are global position coordinates with the axis of symmetry along the z axis. Along the element boundary, Eq. (2) reduces to a linear profile; this assures interelement continuity of the temperature profile. Instead of global coordinates, local coordinates (ξ, η) will be used to define the element temperature profile (see Fig. 2). The origin of the local coordinate system is at the quarter point $[z = 0.25(z_1 + z_2 + z_3 + z_4)$ and $r = 0.25(r_1 + r_2 + r_3 + r_4)]$ with both ξ and η in the range $-1 \le (\xi, \eta) \le 1$. At this point, we will introduce matrix notation for convenience. In terms of local coordinates, the temperature at any arbitrary point (ξ, η) is related to the four nodal values by

$$T(\xi, \eta) = [N_1 N_2 N_3 N_4] \begin{bmatrix} T_1 \\ T_2 \\ T_3 \\ T_4 \end{bmatrix}^{(e)} \tag{3}$$

where the four N_i are defined by

$$N_i(\xi, \eta) = \tfrac{1}{4}(1 + \xi_i \xi)(1 + \eta_i \eta) \tag{4}$$

where $\xi_i = (-1, 1, 1, -1)$ and $\eta_i = (-1, -1, 1, 1)$ for $i = 1, 2, 3, 4$. Note that the shape functions have the unique property that

$$N_i(\xi_j, \eta_j) = \delta_{ij} \tag{5}$$

The global coordinates (z, r) are related to the local coordinates through the element shape functions in a manner analogous to Eq. (3):

$$z(\xi, \eta) = [N_1 N_2 N_3 N_4] \begin{bmatrix} z_1 \\ z_2 \\ z_3 \\ z_4 \end{bmatrix}^{(e)} \tag{6}$$

$$r(\xi, \eta) = [N_1 N_2 N_3 N_4] \begin{bmatrix} r_1 \\ r_2 \\ r_3 \\ r_4 \end{bmatrix}^{(e)} \tag{7}$$

In the work that follows, the chain rule will be used to relate derivatives in the two coordinate systems:

$$\frac{\partial}{\partial \xi} = \frac{\partial z}{\partial \xi}\frac{\partial}{\partial z} + \frac{\partial r}{\partial \xi}\frac{\partial}{\partial r}$$

$$\frac{\partial}{\partial \eta} = \frac{\partial z}{\partial \eta}\frac{\partial}{\partial z} + \frac{\partial r}{\partial \eta}\frac{\partial}{\partial r}$$

In matrix notation, this becomes

$$\begin{bmatrix} \frac{\partial}{\partial \xi} \\ \frac{\partial}{\partial \eta} \end{bmatrix} = \begin{bmatrix} \frac{\partial z}{\partial \xi} & \frac{\partial r}{\partial \xi} \\ \frac{\partial z}{\partial \eta} & \frac{\partial r}{\partial \eta} \end{bmatrix} \begin{bmatrix} \frac{\partial}{\partial z} \\ \frac{\partial}{\partial r} \end{bmatrix} = [J] \begin{bmatrix} \frac{\partial}{\partial z} \\ \frac{\partial}{\partial r} \end{bmatrix} \tag{8}$$

$$[G] = [J]^{-1} = \frac{1}{Det[J]} \begin{bmatrix} \frac{\partial r}{\partial \eta} & \frac{\partial r}{\partial \xi} \\ \frac{\partial z}{\partial \eta} & \frac{\partial z}{\partial \xi} \end{bmatrix} \quad \text{or} \quad [J] = \begin{bmatrix} \frac{\partial z}{\partial \xi} & \frac{\partial r}{\partial \xi} \\ \frac{\partial z}{\partial \eta} & \frac{\partial r}{\partial \eta} \end{bmatrix} \tag{9}$$

The inverse relationship of Eq. (8) is more useful for the analysis that follows:

$$\begin{bmatrix} \frac{\partial}{\partial z} \\ \frac{\partial}{\partial r} \end{bmatrix} = [J]^{-1} \begin{bmatrix} \frac{\partial}{\partial \xi} \\ \frac{\partial}{\partial \eta} \end{bmatrix} \tag{10}$$

Using Eqs. (10) and (3), the elements of the global temperature gradient can be written as

$$\begin{bmatrix} \frac{\partial T}{\partial z} \\ \frac{\partial T}{\partial r} \end{bmatrix} = [J]^{-1} \begin{bmatrix} \frac{\partial N_1}{\partial \xi} & \frac{\partial N_2}{\partial \xi} & \frac{\partial N_3}{\partial \xi} & \frac{\partial N_4}{\partial \xi} \\ \frac{\partial N_1}{\partial \eta} & \frac{\partial N_2}{\partial \eta} & \frac{\partial N_3}{\partial \eta} & \frac{\partial N_4}{\partial \eta} \end{bmatrix} \begin{bmatrix} T_1 \\ T_2 \\ T_3 \\ T_4 \end{bmatrix}^{(e)} = [J]^{-1}[D][T]^e \tag{11}$$

where $[T]^e$ is the element temperature vector. The derivative of the shape functions can be evaluated from Eq. (4).

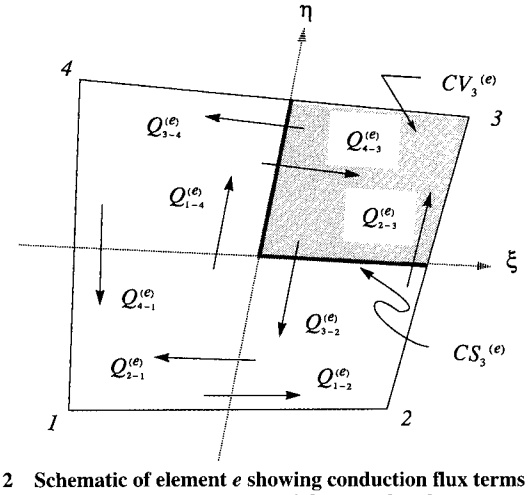

Fig. 2 Schematic of element e showing conduction flux terms and the contribution of element e to partial control volume surrounding node 3.

B. Area Vector over Control Surfaces

As one integrates the variation of the conduction flux over the bounding surfaces of the control volume, Eq. (1) indicates that we require an expression for the differential area $d\boldsymbol{A}$ normal to the surface of the control volume. Following the analysis of Schneider and Zedan[6] for planar geometries, a vector normal to the control volume boundary can be written as

$$d\boldsymbol{S} = dr\boldsymbol{n}_z - dz\boldsymbol{n}_r \tag{12}$$

where $\boldsymbol{n}_z$ and $\boldsymbol{n}_r$ are unit vectors in the z and r directions, respectively. The differential area can be written as

$$d\boldsymbol{A} = 2\pi r(dr\boldsymbol{n}_z - dz\boldsymbol{n}_r) = 2\pi r \begin{bmatrix} dr \\ -dz \end{bmatrix} \tag{13}$$

From the chain rule

$$\begin{bmatrix} dr \\ -dz \end{bmatrix} = \begin{bmatrix} \frac{\partial r}{\partial \eta} & -\frac{\partial r}{\partial \xi} \\ -\frac{\partial z}{\partial \eta} & -\frac{\partial z}{\partial \xi} \end{bmatrix} \begin{bmatrix} d\eta \\ -d\xi \end{bmatrix} \tag{14}$$

or, taking the transpose of Eq. (14) and using Eq. (9)

$$[dr \ -dz] = [d\eta \ -d\xi] \begin{bmatrix} \frac{\partial r}{\partial \eta} & -\frac{\partial z}{\partial \eta} \\ -\frac{\partial r}{\partial \xi} & \frac{\partial z}{\partial \xi} \end{bmatrix} \tag{15}$$

$$= [d\eta \ -d\xi]Det[J][G]^T \tag{16}$$

The final expression for the differential area in matrix form becomes

$$[dA]^T = 2\pi r[dr \ -dz] = 2\pi r[d\eta \ -d\xi]Det[J][G]^T \tag{17}$$

We are now ready to compute the heat conducted across a control volume boundary.

C. Net Heat Conduction

In order to evaluate the conduction term in Eq. (1), we will first develop a general expression of Fourier's Law in matrix form. $\dot{\boldsymbol{q}}$ can be written as

$$\dot{\boldsymbol{q}} = \begin{bmatrix} \dot{q}_z \\ \dot{q}_r \end{bmatrix} = -\begin{bmatrix} k_{zz}k_{zr} \\ k_{rz}k_{rr} \end{bmatrix} \begin{bmatrix} \frac{\partial T}{\partial z} \\ \frac{\partial T}{\partial r} \end{bmatrix}^{(e)} = -[k][J]^{-1}[D] \begin{bmatrix} T_1 \\ T_2 \\ T_3 \\ T_4 \end{bmatrix}^{(e)} \tag{18}$$

where $[k]$ is the thermal conductivity tensor. The rate of conduction heat transfer across an area $d\boldsymbol{A}$ is

$$d\dot{Q} = d\boldsymbol{A} \cdot \dot{\boldsymbol{q}} = [dA]^T[\dot{q}] = -2\pi r Det[J][G]^T[k][G][D] \begin{bmatrix} T_1 \\ T_2 \\ T_3 \\ T_4 \end{bmatrix}^{(e)} \tag{19}$$

Let us now return to Fig. 2, the representative quadrilateral element. Within this element, there are only four different control volume boundaries and corresponding element heat flow terms:

$$\begin{array}{rrl} -1 \le \xi \le 0 & \eta = 0 & \dot{Q}^{(e)}_{1-4} \\ \xi = 0 & -1 \le \eta \le 0 & \dot{Q}^{(e)}_{2-1} \\ 0 \le \xi \le 1 & \eta = 0 & \dot{Q}^{(e)}_{3-2} \\ \xi = 0 & 0 \le \eta \le 1 & \dot{Q}^{(e)}_{4-3} \end{array}$$

These four conduction heat flow terms can be expressed as

$$\begin{aligned} \dot{Q}^{(e)}_{1-4} &= \int_{\xi=0}^{-1} (d\boldsymbol{A} \cdot \dot{\boldsymbol{q}}|_{\eta=0}) = \int_{\xi=0}^{-1} d\dot{Q}^{(e)}_{1-4}|_{\eta=0} \\ \dot{Q}^{(e)}_{2-1} &= \int_{\eta=0}^{-1} (d\boldsymbol{A} \cdot \dot{\boldsymbol{q}}|_{\xi=0}) = \int_{\eta=0}^{-1} d\dot{Q}^{(e)}_{2-1}|_{\xi=0} \\ \dot{Q}^{(e)}_{3-2} &= \int_{\xi=0}^{1} (d\boldsymbol{A} \cdot \dot{\boldsymbol{q}}|_{\eta=0}) = \int_{\xi=0}^{1} d\dot{Q}^{(e)}_{3-2}|_{\eta=0} \\ \dot{Q}^{(e)}_{4-3} &= \int_{\eta=0}^{1} (d\boldsymbol{A} \cdot \dot{\boldsymbol{q}}|_{\xi=0}) = \int_{\eta=0}^{1} d\dot{Q}^{(e)}_{4-3}|_{\xi=0} \end{aligned} \tag{20}$$

An energy balance [Eq. (1)] requires that we determine the net heat conducted out of a control volume. Let $\dot{Q}^{(e)}_i$ represent the net heat conducted across the boundaries of control volume i that lie in element e; the vector of the four *net* conduction tems can be written in terms of the four element heat flow terms as

$$\begin{bmatrix} \dot{Q}^{(e)}_1 \\ \dot{Q}^{(e)}_2 \\ \dot{Q}^{(e)}_3 \\ \dot{Q}^{(e)}_4 \end{bmatrix} = \begin{bmatrix} \dot{Q}^{(e)}_{1-4} - \dot{Q}^{(e)}_{2-1} \\ \dot{Q}^{(e)}_{2-1} - \dot{Q}^{(e)}_{3-2} \\ \dot{Q}^{(e)}_{3-2} - \dot{Q}^{(e)}_{4-3} \\ \dot{Q}^{(e)}_{4-3} - \dot{Q}^{(e)}_{1-4} \end{bmatrix} \tag{21}$$

After numerically performing the integration indicated in Eq. (20), the element conduction matrix for the FCVM can be written symbolically as

$$\begin{bmatrix} \dot{Q}_1 \\ \dot{Q}_2 \\ \dot{Q}_3 \\ \dot{Q}_4 \end{bmatrix}^{(e)} = \begin{bmatrix} K_{11}K_{12}K_{13}K_{14} \\ K_{21}K_{22}K_{23}K_{24} \\ K_{31}K_{32}K_{33}K_{34} \\ K_{41}K_{42}K_{43}K_{44} \end{bmatrix}^{(e)} \begin{bmatrix} T_1 \\ T_2 \\ T_3 \\ T_4 \end{bmatrix}^{(e)} \tag{22}$$

which is similar in form to the FEM.

In the FEM, the element conduction matrix (stiffness matrix) is symmetric. However, this is not the case with the FCVM. On physical grounds, one can argue that the FCVM should not, in general, produce a symmetric element conduction matrix. Consider the two terms K_{12} and K_{21} where

$$\begin{aligned} K^{(e)}_{12} &= \frac{\partial \dot{Q}^{(e)}_1}{\partial T_2} \\ K^{(e)}_{21} &= \frac{\partial \dot{Q}^{(e)}_2}{\partial T_1} \end{aligned} \tag{23}$$

Physically, K_{ij} represents the incremental change in $\dot{Q}^{(e)}_i$ for an incremental change in T_j. Unless there is geometrical similarity (symmetry) between partial control volumes 1 and 2, then there is no reason to expect symmetry.

When the equation analogous to Eq. (22) is developed for the FEM, the terms no longer have the physical significance of conduction heat flow across the control volume boundaries. This is because the governing partial differential equation has been multiplied by a weighting function before integration is performed. This weighting function produces a symmetric element conduction matrix as well as a symmetric global coefficient matrix. If a direct solver is used to solve the resulting algebraic equations, the FCVM will have greater storage requirements than the FEM because of the lack of symmetry.

Hogan[3] has shown analytically that for three node triangular elements and planar geometry, the Galerkin FEM and FCVM have identical element conduction matrices. Computational experiments for steady-state problems with no sources and specified temperature boundary conditions indicate that the two methods produce nearly identical results for planar geometries with four-node quad elements. However, the FEM and FCVM methods have different element capacitance matrices for both three-node triangle and four-node quad elements.

Next, we will develop the element capacitance matrix for an arbitrary four-node quadrilateral.

D. Element Capacitance Matrix

The capacitance effects for an axisymmetric geometry can be written as

$$\frac{\partial}{\partial t}\int_{CV} \rho C_p T(\xi, \eta) 2\pi r(\xi, \eta)\, dr\, dz \tag{24}$$

As with the conduction terms, it is advantageous to perform the desired integration over an element, using local coordinates instead of global coordinates. In Fig. 2, the capacitance contribution of element e to the energy balance around node 3 can be written as

$$(\rho C_p)^{(e)} \frac{\partial}{\partial t}\int_{\eta=0}^{1}\int_{\xi=0}^{1} rT 2\pi Det[J]\, d\xi\, d\eta \tag{25}$$

where the volumetric heat capacity is assumed to be constant for an element. Utilizing the temperature interpolation function Eq. (3), Eq. (25) can be written as

$$2\pi(\rho C_p)^{(e)} \frac{\partial}{\partial t}\int_{\eta=0}^{1}\int_{\xi=0}^{1} r(\xi, \eta) Det[J] \cdot [N_1 N_2 N_3 N_4] \begin{bmatrix} T_1 \\ T_2 \\ T_3 \\ T_4 \end{bmatrix}^{(e)} d\xi\, d\eta \tag{26}$$

Expressions similar to Eq. (26) can be developed for the other three quadrants of element e. The capacitance contribution of element e can be written symbolically as

$$\begin{bmatrix} E_1 \\ E_2 \\ E_3 \\ E_4 \end{bmatrix}^{(e)}_{\text{cap}} = 2\pi(\rho C_p)^{(e)} \begin{bmatrix} C_{11}C_{12}C_{13}C_{14} \\ C_{21}C_{22}C_{23}C_{24} \\ C_{31}C_{32}C_{33}C_{34} \\ C_{41}C_{42}C_{43}C_{44} \end{bmatrix}^{(e)} \begin{bmatrix} T_1 \\ T_2 \\ T_3 \\ T_4 \end{bmatrix}^{(e)} \tag{27}$$

where the terms of the element capacitance matrix are computed from

$$C_{ij}^{(e)} = \int_{CV_i^{(e)}} r(\xi, \eta) Det[J] N_j(\xi, \eta)\, d\xi\, d\eta \tag{28}$$

with $i, j = 1, 2, 3, 4$. The analogous term in the FEM is the mass matrix. The quantity $CV_i^{(e)}$ represents the portion of the control volume surrounding node i in element e; this is termed a partial control volume. The integrals in Eq. (28) are evaluated numerically.

Next, we will evaluate the energy source term for a typical four-node quadrilateral element.

E. Energy Source Term

Following Patankar,[12] we will assume that the energy generation rate per unit volume is linearly dependent on temperature

$$\dot{e}''' = S_P T + S_C \tag{29}$$

where S_P and S_C are constants. We will first work out the contribution of $CV_3^{(e)}$ in element e and then generalize the results for all nodes. By analogy with Eq. (25)

$$\int_{CV_3^{(e)}} \dot{e}'''\, dV = 2\pi \int_{\eta=0}^{1}\int_{\xi=0}^{1} r(S_P T + S_C) Det[J]\, d\xi\, d\eta$$

$$= 2\pi S_P \int_{\eta=0}^{1}\int_{\xi=0}^{1} r(\xi, \eta) T(\xi, \eta) Det[J]\, d\xi\, d\eta$$

$$+ 2\pi S_C \int_{\eta=0}^{1}\int_{\xi=0}^{1} r(\xi, \eta) Det[J]\, d\xi\, d\eta \tag{30}$$

The first integral above is identical in form to the capacitance integral; hence, it is not necessary to redevelop it. The second integral is a product of a centroidal length and area and is evaluated by numerical integration.

To evaluate the contribution of the other three quadrants of element e, just change the integration limits in Eq. (30). The element energy generation can be represented by

$$\begin{bmatrix} E_1 \\ E_2 \\ E_3 \\ E_4 \end{bmatrix}^{(e)}_{\text{source}} = 2\pi S_P \begin{bmatrix} C_{11}C_{12}C_{13}C_{14} \\ C_{21}C_{22}C_{23}C_{24} \\ C_{31}C_{32}C_{33}C_{34} \\ C_{41}C_{42}C_{43}C_{44} \end{bmatrix}^{(e)} \begin{bmatrix} T_1 \\ T_2 \\ T_3 \\ T_4 \end{bmatrix}^{(e)} + 2\pi S_C \begin{bmatrix} \bar{r}_1 A_1 \\ \bar{r}_2 A_2 \\ \bar{r}_3 A_3 \\ \bar{r}_4 A_4 \end{bmatrix}^{(e)} \tag{31}$$

where the C_{ij} are defined by Eq. (28) and

$$\bar{r}_i A_i = \int_{A_i^{(e)}} r(\xi, \eta) Det[J]\, d\xi\, d\eta \tag{32}$$

In the next section, a variety of practical boundary conditions will be considered.

III. Boundary Conditions

If the FCVM is to be useful in solving engineering problems, it must be capable of handling a variety of realistic boundary conditions. The next sections address specified heat flux, aerodynamic heating, convection, and radiation boundary conditions.

A. Specified Heat Flux Boundary Condition

We will start our boundary condition development with the specified heat flux boundary condition. For this case, two logical choices for how to apply this boundary condition include using nodal fluxes or element fluxes. The nodal approach could assume that the heat flux is associated with a surface node. A distribution of flux could be achieved by suitable interpolation between adjacent surface nodes. The simplest nodal interpolation scheme would be to assume a constant nodal flux on each side of the surface node as shown in Fig. 3a. The next level of complexity would be linear interpolation between adjacent nodal values.

For the element flux specification method, the heat flux is assumed to be a constant over the exposed element face. This approach is shown schematically in Fig. 3b. The element flux method was chosen for this work. The energy balance on surface node i (Fig. 3b) will involve contributions from elements e and $e + 1$. In order for the boundary condition treatment to be consistent with the "element assembly" approach of this article, attention will be focused on the contribution of the boundary condition along an element face. First, we will compute the flux leaving the boundary portion of element e that is associated with node i. If $\dot{q}^{(e)}$ is the heat flux leaving the boundary, then the total heat leaving this portion of the boundary is given by

$$\dot{Q}_i^{(e)} = \int_{S_i^{(e)}} \dot{q}^{(e)} 2\pi r\, ds \tag{33}$$

where s is a coordinate measured along the i-j boundary of element e, and $S_i^{(e)}$ is that portion of the boundary of the

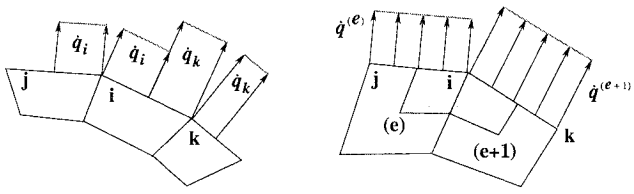

a) Nodal flux b) Element flux

Fig. 3 Two methods of specifying boundary flux.

element that is associated with node i. In Fig. 3b, the i-j boundary is taken to be the line $\eta = 1$; consequently, the i-j boundary corresponds to $-1 \leq \xi \leq 1$. It will be convenient (though not necessary) to express Eq. (33) in local coordinates and evaluate the integral analytically. The result is

$$\dot{Q}_i^{(e)} = 2\pi \frac{S_{ij}^{(e)}}{2} \dot{q}^{(e)} \int_0^1 \frac{1}{2} [(1 + \xi)r_i + (1 - \xi)r_j] \, d\xi$$

$$= 2\pi \frac{S_{ij}^{(e)}}{2} \dot{q}^{(e)} \left(\frac{3}{4} r_i + \frac{1}{4} r_j\right) \tag{34}$$

where $S_{ij}^{(e)} = S_i^{(e)} + S_j^{(e)}$ is the length of the element side i-j, and $\dot{q}^{(e)}$ is an element flux (independent of position). (This result could be written down by utilizing the Theorem of Pappus.) The grouping of terms $(\frac{3}{4} r_i + \frac{1}{4} r_j)$ is the radius at the midpoint of the interval $0 \leq \xi \leq 1$.

$$\tfrac{3}{4}r_i + \tfrac{1}{4}r_j = \tfrac{1}{2}[\tfrac{1}{2}(r_i + r_j) + r_i] = \tfrac{1}{2}(r_i + r_j) + \tfrac{1}{4}(r_i - r_j)$$

A similar integration over the interval $-1 \leq \xi \leq 0$ yields

$$\dot{Q}_j^{(e)} = 2\pi \left(\frac{S_{ij}^{(e)}}{2}\right) \dot{q}^{(e)} \left(\frac{1}{4} r_i + \frac{3}{4} r_j\right) \tag{35}$$

Equations (34) and (35) can be put in a symbolic matrix form to represent the specified flux boundary condition contribution of element e

$$\begin{bmatrix} \dot{Q}_i \\ \dot{Q}_j \end{bmatrix}_{\text{flux}}^{(e)} = 2\pi \frac{S_{ij}^{(e)}}{2} \dot{q}^{(e)} \begin{bmatrix} \frac{3}{4} & \frac{1}{4} \\ \frac{1}{4} & \frac{3}{4} \end{bmatrix} \begin{bmatrix} r_i \\ r_j \end{bmatrix}^{(e)} \tag{36}$$

Equation (36) can be written in a form that allows one to separate out the boundary contribution into a "planar like" portion plus an "axisymmetric modification"

$$\begin{bmatrix} \dot{Q}_i \\ \dot{Q}_j \end{bmatrix}_{\text{flux}}^{(e)} = 2\pi \frac{S_{ij}^{(e)}}{2} \dot{q}^{(e)} \frac{1}{2} (r_i + r_j)$$

$$\cdot \left\{ \begin{bmatrix} 1 \\ 1 \end{bmatrix} - \frac{r_j - r_i}{2(r_i + r_j)} \begin{bmatrix} 1 \\ -1 \end{bmatrix} \right\} \tag{37}$$

Since the above results are independent of the element temperature vector, only the right side of the global matrix must be modified to account for a specified heat flux boundary condition.

B. Aerodynamic Heating Boundary Condition

For aerodynamic heating, the heat flux is assumed given as the product of a transfer coefficient times a recovery enthalpy driving potential

$$\dot{q}^{(e)} = C_h^{(e)}(i_w - i_r) \tag{38}$$

where $C_h^{(e)}$ is the element transfer coefficient. Hence, the element e contribution to the energy balance on node i is given by

$$\dot{Q}_i^{(e)} = C_h^{(e)} \int_{S_i^{(e)}} (i_w - i_r) 2\pi r \, ds \tag{39}$$

It will be assumed that the wall enthalpy varies linearly with position:

$$i_w = \tfrac{1}{2}(1 + \xi)i_i + \tfrac{1}{2}(1 - \xi)i_j = \tfrac{1}{2}(i_i + i_j) + \tfrac{1}{2}(i_j - i_i)\xi \tag{40}$$

After performing the integration indicated by Eq. (39), the element aerodynamic heating matrix at time $n + 1$ can be written as

$$\begin{bmatrix} \dot{Q}_i \\ \dot{Q}_j \end{bmatrix}_{\text{aero}}^{(e)} = 2\pi \frac{S_{ij}^{(e)}}{2} C_h^{(e)} \frac{1}{2} (r_i + r_j) \left\{ \begin{bmatrix} \frac{3}{4} & \frac{1}{4} \\ \frac{1}{4} & \frac{3}{4} \end{bmatrix} \begin{bmatrix} i_i^{n+1} \\ i_j^{n+1} \end{bmatrix} \right.$$

$$\left. - \begin{bmatrix} i_r \\ i_r \end{bmatrix} + \frac{(r_j - r_i)}{2(r_j + r_i)} \left\{ \begin{bmatrix} -\frac{5}{6} & -\frac{1}{6} \\ \frac{1}{6} & \frac{5}{6} \end{bmatrix} \begin{bmatrix} i_i^{n+1} \\ i_j^{n+1} \end{bmatrix} - \begin{bmatrix} -i_r \\ i_r \end{bmatrix} \right\} \right\} \tag{41}$$

where the $n + 1$ superscript denotes the current time step. Note that the recovery enthalpy is evaluated at the $n + 1$ time step.

Unfortunately, Eq. (41) is in terms of nodal enthalpy instead of nodal temperature. In order to avoid iteration because of the possible nonlinear relationship between temperature and enthalpy, we will expand the enthalpy in a Taylor series in time:

$$i_i^{n+1} = i_i^n + \frac{\partial i_i}{\partial T} (T_i^{n+1} - T_i^n) = i_i^n + C_{P_i}(T_i^{n+1} - T_i^n) \tag{42}$$

Substituting Eq. (42) into Eq. (41) and simplifying, the element aerodynamic heating matrix becomes

$$\begin{bmatrix} \dot{Q}_i \\ \dot{Q}_j \end{bmatrix}_{\text{aero}}^{(e)} = 2\pi \frac{S_{ij}^{(e)}}{2} C_h^{(e)} \frac{1}{2} (r_i + r_j) \left\{ \begin{bmatrix} \frac{3}{4} C_{P_i} & \frac{1}{4} C_{P_j} \\ \frac{1}{4} C_{P_i} & \frac{3}{4} C_{P_j} \end{bmatrix}^{(e)} \right.$$

$$\cdot \begin{bmatrix} T_i^{n+1} \\ T_j^{n+1} \end{bmatrix}^{(e)} - \begin{bmatrix} i_r^{n+1} + \frac{3}{4}(C_{P_i}T_i^n - i_i^n) + \frac{1}{4}(C_{P_j}T_j^n - i_j^n) \\ i_r^{n+1} + \frac{1}{4}(C_{P_i}T_i^n - i_i^n) + \frac{3}{4}(C_{P_j}T_j^n - i_j^n) \end{bmatrix}$$

$$+ \frac{(r_j - r_i)}{2(r_j + r_i)} \left\{ \begin{bmatrix} -\frac{5}{6} C_{P_i} & -\frac{1}{6} C_{P_j} \\ \frac{1}{6} C_{P_i} & \frac{5}{6} C_{P_j} \end{bmatrix}^{(e)} \begin{bmatrix} T_i^{n+1} \\ T_j^{n+1} \end{bmatrix}^{(e)} \right.$$

$$\left. \left. - \begin{bmatrix} -i_r^{n+1} + \frac{5}{6}(C_{P_i}T_i^n - i_i^n) + \frac{1}{6}(C_{P_j}T_j^n - i_j^n) \\ i_r^{n+1} - \frac{1}{6}(C_{P_j}T_i^n - i_i^n) - \frac{5}{6}(C_{P_i}T_j^n - i_j^n) \end{bmatrix} \right\} \right\} \tag{43}$$

Equation (43) is in a useful computational form since the unknown temperature vector at time $n + 1$ appears explicitly. The coefficient of the element temperature vector in Eq. (43) will be used to modify the left hand side of the global matrix; all other terms in Eq. (43) modify the right side vector. Note that i_r is an element variable, independent of position but possibly time dependent.

C. Convective Boundary Condition

For traditional convection, Eq. (38) is replaced with

$$\dot{q}^{(e)} = h^{(e)}(T_w - T_\infty) \tag{44}$$

The element convection matrix can be derived by analogy from Eq. (41) for aerodynamic heating by simply replacing i by C_PT, and C_pC_h by h

$$\begin{bmatrix} \dot{Q}_i \\ \dot{Q}_j \end{bmatrix}^{(e)}_{\text{conv}} = 2\pi \frac{S_{ij}^{(e)}}{2} h^{(e)} \frac{1}{2}(r_i + r_j) \left\{ \begin{bmatrix} \frac{3}{4} & \frac{1}{4} \\ \frac{1}{4} & \frac{3}{4} \end{bmatrix} \begin{bmatrix} T_i^{n+1} \\ T_j^{n+1} \end{bmatrix} - \begin{bmatrix} T_\infty \\ T_\infty \end{bmatrix} + \frac{(r_j - r_i)}{2(r_j + r_i)} \left\{ \begin{bmatrix} -\frac{5}{6} & -\frac{1}{6} \\ \frac{1}{6} & \frac{5}{6} \end{bmatrix} \begin{bmatrix} T_i^{n+1} \\ T_j^{n+1} \end{bmatrix} - \begin{bmatrix} -T_\infty \\ T_\infty \end{bmatrix} \right\} \right\} \tag{45}$$

All temperatures in Eq. (45) are evaluated at the $n + 1$ time step.

D. Radiation Boundary Condition

Assume that the radiative heat flux leaving the side of an element is given by

$$\dot{q}^{(e)}_{\text{rad}} = \varepsilon^{(e)} \sigma F^{(e)} (T^4 - T_r^4) \tag{46}$$

where $\varepsilon^{(e)}$ is the element emittance, $F^{(e)}$ is the view factor between element e and its surroundings at temperature T_r (independent of position). The element radiative flux matrix for boundary i-j is given by

$$\begin{bmatrix} \dot{Q}_i \\ \dot{Q}_j \end{bmatrix}^{(e)}_{\text{rad}} = \varepsilon^{(e)} \sigma F^{(e)} \begin{bmatrix} \int_{S_i^{(e)}} (T^4 - T_r^4) 2\pi r \, ds \\ \int_{S_j^{(e)}} (T^4 - T_r^4) 2\pi r \, ds \end{bmatrix} \tag{47}$$

In order to perform the integration in Eq. (47) analytically, the temperature profile along the boundary of the element can be written as

$$\begin{aligned} T(\xi) &= \tfrac{1}{2}(1 + \xi) T_i + \tfrac{1}{2}(1 - \xi) T_j \\ &= \tfrac{1}{2}(T_i + T_j) + \tfrac{1}{2}(T_j - T_i)\xi \end{aligned} \tag{48}$$

The relationship $r(\xi)$ has already been given in Eq. (34). Although the analytical integration of Eq. (47) is straightforward, it is lengthy and the details will be omitted. An intermediate result is

$$\begin{bmatrix} \dot{Q}_i \\ \dot{Q}_j \end{bmatrix}^{(e)}_{\text{rad}} = 2\pi \varepsilon^{(e)} \sigma F^{(e)} \frac{S_{ij}^{(e)}}{2} \frac{1}{2}(r_i + r_j) \cdot \left\{ \begin{bmatrix} \bar{T}_i^4 - T_r^4 \\ \bar{T}_j^4 - T_r^4 \end{bmatrix} - \frac{(r_j - r_i)}{2(r_j + r_i)} \begin{bmatrix} \hat{T}_i^4 - T_r^4 \\ \hat{T}_j^4 - T_r^4 \end{bmatrix} \right\} \tag{49}$$

where the following effective temperatures are defined as:

$$\left.\begin{aligned} \bar{T}_i^4 &= \tfrac{1}{5}(\bar{T}^4 + \bar{T}^3 T_i + \bar{T}^2 T_i^2 + \bar{T} T_i^3 + T_i^4) \\ \hat{T}_i^4 &= \tfrac{1}{15}(\bar{T}^4 + 2\bar{T}^3 T_i + 3\bar{T}^2 T_i^2 + 4\bar{T} T_i^3 + 5T_i^4) \\ \bar{T} &= \tfrac{1}{2}(T_i + T_j) \end{aligned}\right\} \tag{50}$$

The results of Eq. (50) are also valid for $i \rightarrow j$. Note that when $T_i = T_j = \bar{T}$, then $\bar{T} = \hat{T}_i = T_i$. Equation (49) is nonlinear in the unknown nodal temperatures. To avoid iteration, a Taylor series linearization in time similar to that used for the aerodynamic heating boundary condition will be utilized. In matrix form

$$\begin{bmatrix} (\bar{T}_i^{n+1})^4 \\ (\bar{T}_j^{n+1})^4 \end{bmatrix} = \begin{bmatrix} (\bar{T}_i^n)^4 \\ (\bar{T}_j^n)^4 \end{bmatrix} + \begin{bmatrix} \frac{\partial \bar{T}_i^4}{\partial T_i} & \frac{\partial \bar{T}_i^4}{\partial T_j} \\ \frac{\partial \bar{T}_j^4}{\partial T_i} & \frac{\partial \bar{T}_j^4}{\partial T_j} \end{bmatrix} \begin{bmatrix} (T_i^{n+1} - T_i^n) \\ (T_j^{n+1} - T_j^n) \end{bmatrix} \tag{51}$$

An analogous result can be derived for $\hat{T}^{n+1}$

$$\begin{bmatrix} (\hat{T}_i^{n+1})^4 \\ (\hat{T}_j^{n+1})^4 \end{bmatrix} = \begin{bmatrix} (\hat{T}_i^n)^4 \\ (\hat{T}_j^n)^4 \end{bmatrix} + \begin{bmatrix} \frac{\partial \hat{T}_i^4}{\partial T_i} & \frac{\partial \hat{T}_i^4}{\partial T_j} \\ \frac{\partial \hat{T}_j^4}{\partial T_i} & \frac{\partial \hat{T}_j^4}{\partial T_j} \end{bmatrix} \begin{bmatrix} (T_i^{n+1} - T_i^n) \\ (T_j^{n+1} - T_j^n) \end{bmatrix} \tag{52}$$

Substituting Eqs. (51) and (52) into Eq. (49), we obtain

$$\begin{aligned} \begin{bmatrix} \dot{Q}_i \\ \dot{Q}_j \end{bmatrix}^{(e)}_{\text{rad}} = 2\pi \varepsilon^{(e)} \sigma F^{(e)} \frac{S_{ij}^{(e)}}{2} \frac{1}{2}(r_i + r_j) \Bigg\{ \Bigg\{ \begin{bmatrix} \frac{\partial \bar{T}_i^4}{\partial T_i} & \frac{\partial \bar{T}_i^4}{\partial T_j} \\ \frac{\partial \bar{T}_j^4}{\partial T_i} & \frac{\partial \bar{T}_j^4}{\partial T_j} \end{bmatrix}^{(n)} \cdot \begin{bmatrix} T_i^{n+1} \\ T_j^{n+1} \end{bmatrix} - \begin{bmatrix} \frac{\partial \hat{T}_i^4}{\partial T_i} & \frac{\partial \hat{T}_i^4}{\partial T_j} \\ \frac{\partial \hat{T}_j^4}{\partial T_i} & \frac{\partial \hat{T}_j^4}{\partial T_j} \end{bmatrix}^{(n)} \begin{bmatrix} T_i^n \\ T_j^n \end{bmatrix} \\ - \begin{bmatrix} T_r^4 - \bar{T}_i^4 \\ T_r^4 - \bar{T}_j^4 \end{bmatrix}^{(n)} \Bigg\} + \frac{(r_j - r_i)}{2\pi(r_j + r_i)} \Bigg\{ \begin{bmatrix} -\frac{\partial \hat{T}_i^4}{\partial T_i} & -\frac{\partial \hat{T}_i^4}{\partial T_j} \\ -\frac{\partial \hat{T}_j^4}{\partial T_i} & -\frac{\partial \hat{T}_j^4}{\partial T_j} \end{bmatrix}^{(n)} \begin{bmatrix} T_i^{n+1} \\ T_j^{n+1} \end{bmatrix} \\ - \begin{bmatrix} -\frac{\partial \hat{T}_i^4}{\partial T_i} & -\frac{\partial \hat{T}_i^4}{\partial T_j} \\ -\frac{\partial \hat{T}_j^4}{\partial T_i} & -\frac{\partial \hat{T}_j^4}{\partial T_j} \end{bmatrix}^{(n)} \begin{bmatrix} T_i^n \\ T_j^n \end{bmatrix} - \begin{bmatrix} T_r^4 - \bar{T}_i^4 \\ T_r^4 - \bar{T}_j^4 \end{bmatrix}^{(n)} \Bigg\} \Bigg\} \end{aligned} \tag{53}$$

This completes the formal development of the boundary conditions for the FCVM.

While the emphasis of this article is on axisymmetric geometries, it should be pointed out that the element boundary condition equations have been written in a form such that the corresponding planar geometry results can be readily written down. For example, in Eq. (53), the factor $2\pi\frac{1}{2}(r_i + r_j)$ is replaced by unity, and the factor $(r_j - r_i)$ is replaced by zero, with the resulting equation being the planar geometry version of the element radiation boundary condition. The same logic can be applied to Eqs. (37), (43), and (45).

IV. Example Calculations

To demonstrate the accuracy of the FCVM, solutions for two axisymmetric example problems are compared with analytical solutions. Additionally, the errors associated with using a skewed mesh are compared with those for a rectangular mesh. For all example calculations presented here, a fully implicit time integration scheme with first-order accuracy was used, and the linear equations were solved using the direct band solver method of Gopalakrishnan and Palaniappan.[13] All calculations reported here were performed on a Sun SPARC station 1™ using double precision.

A. Cylinder with Specified Heat Flux on One End (Rectangular Mesh)

Figure 4 shows the geometry, material properties, and boundary conditions for this example problem. This problem is equivalent to a one-dimensional planar geometry with one insulated and one specified heat flux boundary condition. Although it is a simple problem, it is important because it evaluates the significance of any assumptions associated with the implementation of the boundary contributions of the radial conduction terms. With an appropriately formulated numerical method, the computed temperatures should vary only in the axial (z) direction.

To evaluate the FCVM solution of this problem, the difference in the computed temperature and the analytical solution is evaluated. The analytical solution is presented in Beck et al.[14] Figure 5 shows the percentage error in the computed surface temperature rise as a function of the number of elements in the axial direction for several Fourier numbers ($\alpha t/L^2$); two elements were used in the radial direction for all calculations. The relative error is defined using

$$\Delta T_{\max} = T(z = 0, t) - T(z = 0, t = 0) \tag{54}$$

as

$$\text{relative error} = (\Delta T_{\max}|_c - \Delta T_{\max}|_a)/\Delta T_{\max}|_a \tag{55}$$

Note that using this definition, the error is indeterminate for the initial conditions ($t = 0$).

As the mesh was refined in the axial (z) direction, $\alpha\Delta t/\Delta z^2$ the mesh Fourier number, was kept constant at unity. For 10 axial elements, $\Delta t = 0.01$ s was used. When the mesh was refined by a factor of two, the time step was reduced by a factor of 4. The results in Fig. 5 demonstrate that 1) temperature errors decrease with increasing dimensionless time, 2) reasonable errors can be obtained even on a coarse mesh, and 3) the error decreases quadratically as the mesh is refined. The computed temperatures are essentially uniform (to six significant digits) in the radial direction suggesting that the formulation of the radial terms is correct.

Figure 5 also presents computational results using the Galerkin FEM[15] with the same number of quadrilateral elements and time integration scheme as the FCV results. The FE errors are uniformly smaller than the FCV results for this example problem. The ratio of FCV-to-FE errors fell in the range of 1.06–1.11 for all the results of Fig. 5; for this example, the two methods are deemed comparable in terms of accuracy.

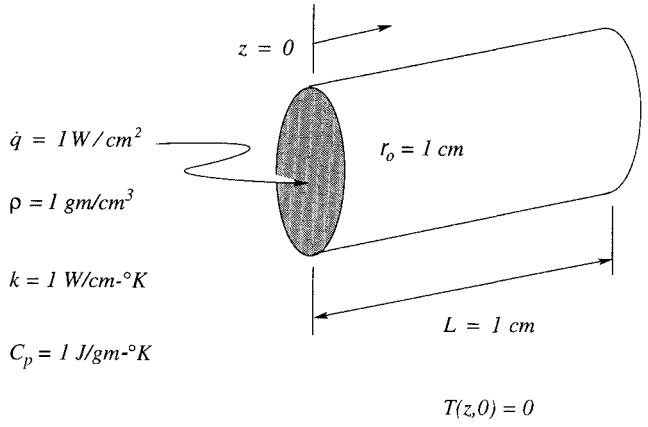

Fig. 4 Boundary conditions and material properties for cylinder with specified heat flux one end.

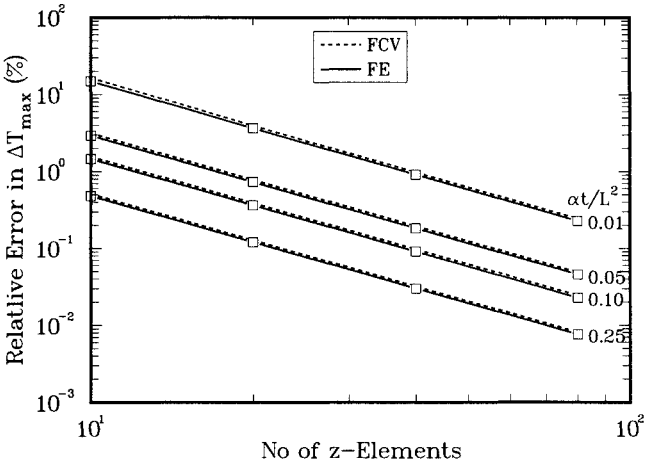

Fig. 5 Variation of relative error in the maximum temperature rise (at the surface) with the number of axial elements ($\alpha\Delta t/\Delta z^2 = 1$) for several Fourier numbers (both FEM and FCVM).

B. Cylinder with Temperature-Dependent Source (Rectangular Mesh)

The second example problem is a solid cylinder with an internal energy generation that varies linearly with temperature. The cylinder is initially at a uniform temperature of 300 K. For $t > 0$, the surface temperature is fixed at 300 K and the cylinder ends are insulated. In this example, the maximum temperature occurs at the centerline of the cylinder. Figure 6 shows a sketch of the geometry and material properties for this example problem.

Figure 7 shows the relative error as a function of time for 10, 20, 40, and 80 elements in the radial direction; two axial elements and $\alpha\Delta t/\Delta r^2 = 1$ were used in all cases. In this example, the relative error is defined using

$$\Delta T_{\max} = T(r = 0, t) - T(r = r_0, t) \tag{56}$$

and Eq. (55). For the initial conditions ($t = 0$), the error defined using Eq. (55) is indeterminate. For these results, a rectangular mesh with two axial elements was used. The analytical solution was developed by the authors for comparison with the computed solution, and is given by

$$\psi = \psi_\infty \frac{J_0(pr/r_0)}{J_0(p)} + 2\sum_{n=1}^{\infty}\left(1 - \frac{\psi_\infty \upsilon_n^2}{(\upsilon_n^2 - p^2)}\right) \cdot \frac{J_0(\upsilon_n r/r_0)}{\upsilon_n J_1(\upsilon_n)} \exp\left(-\frac{(\upsilon_n^2 - p^2)\alpha t}{r_0^2}\right) \tag{57}$$

where

$$\psi = \frac{1 + \alpha_0(T - T_0)}{1 + \alpha_0(T_i - T_0)} \qquad p^2 = \frac{\alpha_0 r_0^2 \dot{e}'''_0}{k} \tag{58}$$

and the eigenvalues are the roots of $J_0(\upsilon_n) = 0$.

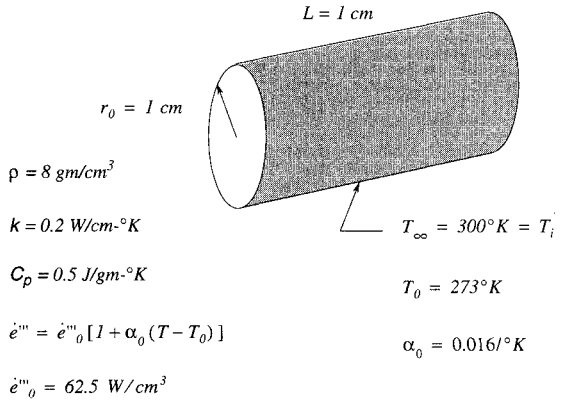

Fig. 6 Sketch of the geometry, material properties, and source term for a solid cylinder with temperature-dependent source.

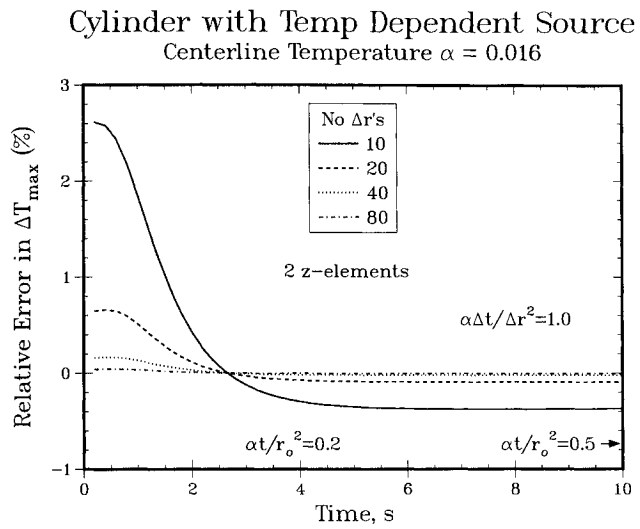

Fig. 7 Relative error in the maximum temperature rise (at the centerline) as a function of time for several meshes.

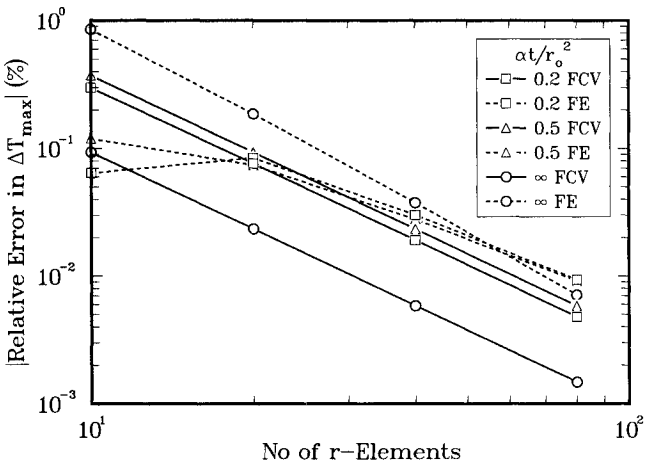

Fig. 8 Relative error in the maximum temperature rise (at the centerline) for temperature-dependent source problem as mesh is refined, $\alpha\Delta t/\Delta r^2 = 1$.

Figure 8 shows the relative error for both the FCVM and FEM as a function of the number of radial elements for Fourier numbers of 0.2, 0.5, and ∞ (t = 4, 10, and ∞ s). For the two finite time values, neither method is uniformly better than the other over the range of radial elements considered. While the FCVM consistently displays quadratic convergence as the mesh is refined, the FEM results are not quadratic. We offer no explanation for this behavior. For the steady-state results, both methods demonstrate quadratic convergence with the FCVM results having an order of magnitude smaller error. This superior performance of the FCVM was found for other steady-state problems. These results demonstrate good accuracy on a coarse mesh and the second-order convergence of the FCVM.

We have demonstrated the validity of the FCVM on simple but meaningful example problems. However, the power of the method lies in the ease with which it can handle geometrically complex objects using a mesh of significant skewness. This will be demonstrated with the final example problem.

C. Cylinder with Temperature-Dependent Source (Skewed Mesh)

To investigate the errors associated with the use of a mesh with poorly shaped elements, the solution was also computed using the elements shown in Fig. 9. In this mesh, there are

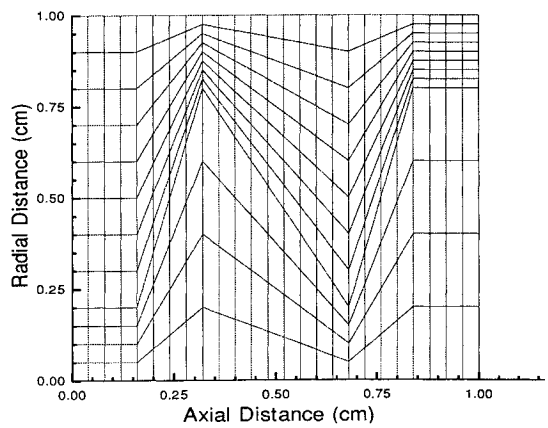

Fig. 9 Skewed mesh used for testing the flexibility and accuracy of the FCVM.

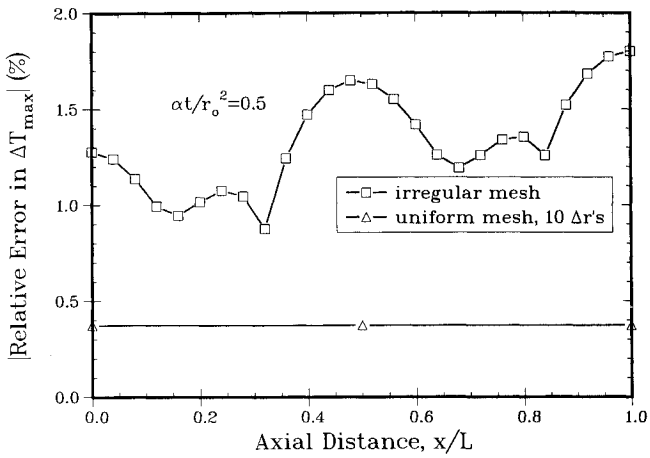

Fig. 10 Relative error in the maximum temperature rise (at the centerline) as a function of axial distance at a time of 10 s for both the rectangular and the skewed meshes.

many poorly shaped elements, as well as some rectangular elements.

Figure 10 shows the relative error in the centerline temperature rise as a function of axial distance at a dimensionless time of $\alpha t/r_0^2 = 0.5$ for both the rectangular mesh (10 equal Δr's) and the skewed mesh. In this example, the relative error is defined by Eqs. (55) and (56). The error is uniform for the rectangular mesh, but varies with axial position for the skewed mesh. There appears to be a correlation between mesh coarseness in the radial direction and error magnitude. The relative errors are smaller in the lower left corner ($r \approx 0$, $z \approx 0$) where the mesh is finer. Near the lower right corner ($r \approx 0$, $z \approx 1$), the mesh is coarser and the relative errors are larger. Both the percentage and the absolute errors are small for the skewed mesh. This example demonstrates the potential for the FCVM for solving geometrically complicated heat conduction problems.

V. Concluding Remarks

We have presented our philosophy of the FCVM and a review of the literature pertaining to this approach. A detailed development of the discretized equations for four-node quadrilateral elements and axisymmetric geometries is presented using terminology familiar to the finite element community. The implementation of the specified heat flux, aerodynamic heating, convective, and radiative boundary conditions is developed in detail. Conceptually, there is no reason the FCVM cannot be applied to three-dimensional problems. The accuracy and flexibility of the FCVM is demonstrated by comparing computed and analytical solutions for axisymmetric,

transient heat conduction problems. Solutions were compared for both rectangular and skewed meshes. The agreement between the computed and analytical solutions was shown to be excellent for the problems we considered, and the method was shown to have quadratic convergence as the mesh was refined. The computed temperature distribution using a highly skewed mesh compared well with the analytical solution. This demonstrates the accuracy, generality, and robustness of the FCVM for solving geometrically complicated heat conduction problems.

Our implementation of this method into a practical computer code (called FCV) provides the following capabilities. Both planar and axisymmetric, two-dimensional, transient, nonlinear, heat conduction problems can be solved. The code accounts for fully anisotropic and temperature-dependent material properties. The specified heat flux, aerodynamic heating, convective, and radiative boundary conditions discussed in this article are included. In addition to these boundary conditions, the capability to solve coupled radiative/conduction heat transfer in enclosures has been implemented. The radiative transfer is formulated using the net radiation method for diffuse gray enclosures.

The FCVM presented in this article can be applied to simulate other physical phenomenon in addition to heat conduction problems. This approach is appealing because it is formulated directly in terms of physically meaningful quantities. For example, this approach has been applied to heat, mass, and incompressible fluid flow using primitive variables by several researchers.[16-18]

Acknowledgments

This work was performed at Sandia National Laboratories and supported by the U.S. Department of Energy under Contract DE-AC04-76DP00789. The authors acknowledge the assistance of R. W. Douglass at the University of Nebraska in developing the analytical solution for the example problem of a solid cylinder with a specified surface temperature and temperature dependent source.

References

[1]Winslow, A. M., "Numerical Solution of the Quasilinear Poisson Equation in a Nonuniform Triangle Mesh," *Journal of Computational Physics*, Vol. 1, No. 2, 1967, pp. 149–172.

[2]Baliga, B. R., "A Control Volume Based Finite Element Method for Convective Heat and Mass Transfer," Ph.D. Dissertation, Mechanical Engineering Dept., Univ. of Minnesota, Minneapolis, MN, 1978.

[3]Hogan, R. E., "Heat Transfer Analysis of Radiant Heating Panels-Hot Water Pipes in Concrete Slab Floor," M.S. Thesis, Mechanical Engineering Dept., LA Tech Univ., Ruston, LA, Aug. 1979.

[4]Hogan, R. E., and Blackwell, B. F., "Comparison of Numerical Model with ASHRAE Design Procedure for Warm Water Concrete Floor Heating Panels," *ASHRAE Transactions*, Vol. 92, Pt. 1, 1986, pp. 589–602.

[5]Ramadhyani, S., and Patankar, S. V., "Solution of the Poisson Equation: Comparison of the Galerkin and Control-Volume Methods," *International Journal for Numerical Methods in Engineering*, Vol. 15, No. 9, 1980, pp. 1395–1402.

[6]Schneider, G. E., and Zedan, M., "Control Volume Based Finite Element Formulation of the Heat Conduction Equation," AIAA/ASME 3rd Joint Thermophysics, Fluids, Plasma and Heat Transfer Conf., AIAA Paper 82-0909, St. Louis, MO, June 7–11, 1982.

[7]Raw, M. J., Schneider, G. E., and Hassani, V., "Development and Evaluation of Nine-Node Quadratic Control Volume Based Finite Element for Heat Conduction Modelling," AIAA 22nd Aerospace Sciences Meeting, AIAA Paper 84-0493, Reno, NV, Jan. 9–12, 1984.

[8]Banaszek, J., "A Conservative Finite Element Method for Heat Conduction Problems," *International Journal for Numerical Methods in Engineering*, Vol. 20, No. 11, 1984, pp. 2033–2050.

[9]Minkowycz, W. J., Sparrow, E. M., Schneider, G. E., and Pletcher, R. H., "Handbook of Numerical Heat Transfer," Wiley-Interscience, New York, 1988, Chaps. 10–11.

[10]Kao, T. K., Hardisty, H., and Wallace, F. J., "An Energy Balance Approach to the Finite Element Method Applied to Heat Transfer Analysis," *International Journal of Mechanical Engineering Education*, Vol. 11, No. 1, 1983, pp. 1–19.

[11]Kettleborough, C. F., private communication, College Station, TX, Jan. 1991.

[12]Patankar, S. V., "Numerical Heat Transfer and Fluid Flow," Hemisphere, Washington, DC, 1980.

[13]Gopopaiakrishnan, T. C., and Palaniappan, A. B., "Band Algorithm for Unsymmetric Matrices in Finite Element and Semi-Discrete Methods," *International Journal for Numerical Methods in Engineering*, Vol. 18, No. 8, 1982, pp. 1197–1211.

[14]Beck, J. V., Blackwell, B., and St. Clair, C. R., Jr., "Inverse Heat Conduction," Wiley, New York, 1985.

[15]Gartling, D. K., "COYOTE—A Finite Element Computer Program for Nonlinear Heat Conduction Problems," Sandia National Lab., SAND77-1332, Albuquerque, NM, Oct. 1982.

[16]Prakash, C., "An Improved Control Volume Finite-Element Method for Heat and Mass Transfer, and for Fluid Flow Using Equal-Order Velocity-Pressure Interpolation," *Numerical Heat Transfer*, Vol. 9, No. 3, 1986, pp. 253–276.

[17]Schneider, G. E., and Raw, M. J., "Control Volume Finite-Element Method for Heat Transfer and Fluid Flow Using Collocated Variables—1. Computational Procedure," *Numerical Heat Transfer*, Vol. 11, No. 4, 1987, pp. 363–390.

[18]Schneider, G. E., and Raw, M. J., "Control Volume Finite-Element Method for Heat Transfer and Fluid Flow Using Collocated Variables—2. Application and Validation," *Numerical Heat Transfer*, Vol. 11, No. 4, 1987, pp. 391–400.